Otero Fumega, Adolfo; Lado, Jose

Moiré-driven multiferroic order in twisted CrCl3, CrBr3 and CrI3 bilayers

Published in:
2D Materials

DOI:
10.1088/2053-1583/acc671

Published: 03/04/2023

Document Version
Publisher's PDF, also known as Version of record

Moiré-driven multiferroic order in twisted $CrCl_3$, $CrBr_3$ and CrI_3 bilayers

To cite this article: Adolfo O Fumega and Jose L Lado 2023 *2D Mater.* **10** 025026

2D Materials

OPEN ACCESS

RECEIVED
12 January 2023

REVISED
13 March 2023

ACCEPTED FOR PUBLICATION
22 March 2023

PUBLISHED
3 April 2023

PAPER

Moiré-driven multiferroic order in twisted $CrCl_3$, $CrBr_3$ and CrI_3 bilayers

Adolfo O Fumega[1,*] **and Jose L Lado**[1,*]

Department of Applied Physics, Aalto University, 02150 Espoo, Finland
* Authors to whom any correspondence should be addressed.

E-mail: adolfo.oterofumega@aalto.fi and jose.lado@aalto.fi

Keywords: multiferroic, 2D magnets, twisted van der Waals, strong magnetoelectric coupling, magnetic skyrmions

Supplementary material for this article is available online

Abstract

Layered van der Waals materials have risen as a powerful platform to engineer artificial competing states of matter. Here we show the emergence of multiferroic order in twisted chromium trihalide bilayers, an order fully driven by the moiré pattern and absent in aligned multilayers. Using a combination of spin models and *ab initio* calculations, we show that a spin texture is generated in the moiré supercell of the twisted system as a consequence of the competition between stacking-dependent interlayer magnetic exchange and magnetic anisotropy. An electric polarization arises associated with such a non-collinear magnetic state due to the spin–orbit coupling, leading to the emergence of a local ferroelectric order following the moiré. Among the stochiometric trihalides, our results show that twisted $CrBr_3$ bilayers give rise to the strongest multiferroic order. We further show the emergence of a strong magnetoelectric coupling, which allows the electric generation and control of magnetic skyrmions. Our results put forward twisted chromium trihalide bilayers, and in particular $CrBr_3$ bilayers, as a powerful platform to engineer artificial multiferroic materials and electrically tunable topological magnetic textures.

1. Introduction

Multiferroic materials display more than one ferroic order at the same time [1–3], and in particular, they can simultaneously host magnetic and ferroelectric orders. The existence of multiple symmetry-breaking orders allows having a coupling between electric and magnetic degrees of freedom [4]. Over the last two decades, a variety of multiferroic bulk compounds has been demonstrated [5–8], providing alternative strategies for multifunctional devices [7, 9]. However, focusing on the realm of two-dimensional (2D) materials, purely 2D multiferroics have remained elusive until the recent demonstration of multiferroic order in NiI_2 [10, 11]. Beyond isolating individual multiferroic monolayers, a potential alternative strategy to realize multiferroic order in van der Waals materials relies on artificially engineering it from originally non-multiferroic monolayers [12]. The electric control of magnetism provided by van der Waals multiferroics would open radically new ways of controlling artificial van der Waals matter [13–25].

The weak bonding between layers in van der Waals materials allows combining monolayers in twisted heterostructures. Monolayer 2D materials can display different symmetry-breaking orders [11, 26–28], constituting a family of minimal building blocks that can be used to artificially engineer other emergent orders. This strategy has been widely exploited to engineer moiré correlated and topological states using 2D materials [13, 16, 17, 29–33]. Recently, this strategy has been extended to 2D magnetic materials including chromium trihalides, leading to a variety of twist-induced magnetic orders [34–41]. However, using twist engineering to realize a multiferroic order has so far remained unexplored.

Here we demonstrate the emergence of a multiferroic state in the family of twisted chromium trihalide CrX_3 (X = Cl, Br and I) bilayers by combining first principles and effective spin Hamiltonians. We first show the emergence of a non-collinear spin texture due to the modulation of the interlayer exchange coupling in the moiré unit cell. Associated with the spin texture an electric polarization emerges as a consequence of spin–orbit coupling

(SOC) and the local magnetic non-collinearity in the moiré domains. Using *ab initio* calculations we extract the value of the electric polarization driven by non-collinear magnetic texture, and demonstrate its dependence on the halide of CrX_3. Therefore, we provide a quantification of the resulting multiferroic order. Furthermore, we analyze the emergent magnetoelectric coupling, demonstrating how it allows us to electrically drive transitions between different topological spin textures employing an interlayer bias.

2. Results and discussion

We start our analysis by describing the magnetic order that emerges in twisted CrX_3 bilayers. The magnetic behavior of CrX_3 monolayers can be described by a spin Hamiltonian in a honeycomb lattice

$$\mathcal{H} = -\frac{J}{2}\sum_{\langle i,j\rangle}\mathbf{S}_i\cdot\mathbf{S}_j - \frac{A_v}{2}\sum_{\langle i,j\rangle}S_i^zS_j^z - A_u\sum_i(S_i^z)^2 + \mathcal{V}, \tag{1}$$

where J is the first neighbor intralayer ferromagnetic exchange, taking a value on the order of 2–3 meV [42–44]. A_v is the anisotropic magnetic exchange. A_u is the single-ion anisotropy, which is dominated by A_v in CrI_3, $CrBr_3$, and competing with A_v in $CrCl_3$ [45]. Our analysis will focus on the anisotropy regime leading to out-of-plane easy axis, that corresponds to CrI_3, $CrBr_3$ and slightly strained $CrCl_3$ [46, 47]. The term $\mathcal{V}$ contains additional contributions that do not qualitatively affect our analysis, including Kitaev exchange [48], biquadratic exchange [49], direct Dzyaloshinskii–Moriya (DM) interaction [50], and dipolar coupling [51].

Considering now two layers of CrX_3 stacked together an interlayer magnetic exchange J_M will arise. A moiré pattern like the one shown in figure 1(a) emerges for twist angles lower than 3°. Depending on the stacking between layers two different regions can be distinguished, monoclinic and rhombohedral. Associated with these different regions the sign of J_M will change, i.e. J_M is ferromagnetic (positive) in the rhombohedric stacking and antiferromagnetic (negative) in the monoclinic one [52–55]. This leads to a modulation of J_M in the moiré supercell like the one shown in figure 1(b) [34–37, 56, 57]. Therefore, to model the twisted CrX_3 bilayer we add the interlayer interaction to the Hamiltonian of equation (1) as

$$\mathcal{H}_{Inter} = -\frac{1}{2}\sum_{i,j}J_M(\mathbf{r}_i,\mathbf{r}_j)\mathbf{S}_i\cdot\mathbf{S}_j, \tag{2}$$

where $J_M(\mathbf{r}_i,\mathbf{r}_j)$ is the site-dependent interlayer exchange [58]. Since CrX_3 is composed of Cr^{3+} with a spin state $S = 3/2$, we can solve in a classical way the spin Hamiltonian for the twisted system [59]. The ground state magnetic order is depicted in figure 2(a). We can see that a non-collinear magnetic texture emerges between ferromagnetic and antiferromagnetic regions in agreement with previous theoretical [38, 39] and experimental results [34–37, 40, 41]. Taking this as the starting point, we now show that in the presence of spin–orbit coupling, this topologically-trivial spin texture leads to the emergence of an electric polarization $\mathbf{P}_{ij}$ between first-neighbor spins in the same layer separated by a distance $\mathbf{r}_{ij}$ due to the inverse DM mechanism [60, 61]

$$\mathbf{P}_{ij} = \alpha\lambda_{SOC}\left(\mathbf{r}_{ij}\times\left(\mathbf{S}_i\times\mathbf{S}_j\right)\right), \tag{3}$$

where λ_{SOC} is a coefficient that controls the strength of the spin–orbit coupling and α is a proportionality constant that depends on the electronic structure and crystal environment, which is similar for the three chromium trihalides. The polarization emerges at the middle point between the two neighboring spins $\mathbf{S}_i$ and $\mathbf{S}_j$. From equation (3) we can clearly see the requirement of non-collinearity and the presence of SOC to produce an electric polarization. For the emerging ground state spin texture of the twisted system (figure 2(a)), the associated electric polarization when SOC is introduced is shown in figure 2(b), with P_z the dominant component. From figures 2(a) and (b), we can observe that an electric polarization emerges in both layers in the areas where the non-collinear spin texture occurs. The polarization emerges locally, and for the ground state spin texture the net electric polarization is zero. Therefore, to analyze the strength of the multiferroic order as a function of the parameters that appear in the spin Hamiltonian, we will consider an average of the electric polarization module $\overline{P}$. The module of the electric polarization in the moiré system associated with the ground state spin texture can be seen in figure 1(c). We can observe there, that the ground state breaks the C_6 symmetry of the original system leading to a C_2 symmetry. The lifted C_6 symmetry stems from a spontaneous symmetry breaking of the ground state due to the ratio between the parameters entering the spin Hamiltonian, analogous to the symmetry breaking associate to stripy magnetic orders. Figure 2(c) shows the average polarization as a function of the maximum interlayer exchange J_M^{max}. At low values, the twisted system behaves like two independent layers, remaining ferromagnetic, no spin texture emerges and consequently, there is no electric polarization. By increasing the interlayer coupling, non-collinearity appears and with it an associated electric polarization in virtue of equation (3). Figure 2(d) shows the average polarization as a function of the anisotropic exchange A_v. At high values, the twisted system tends to align the magnetic moments out of the plane. Therefore, no spin texture occurs and thus there is no electric polarization. This situation happens for

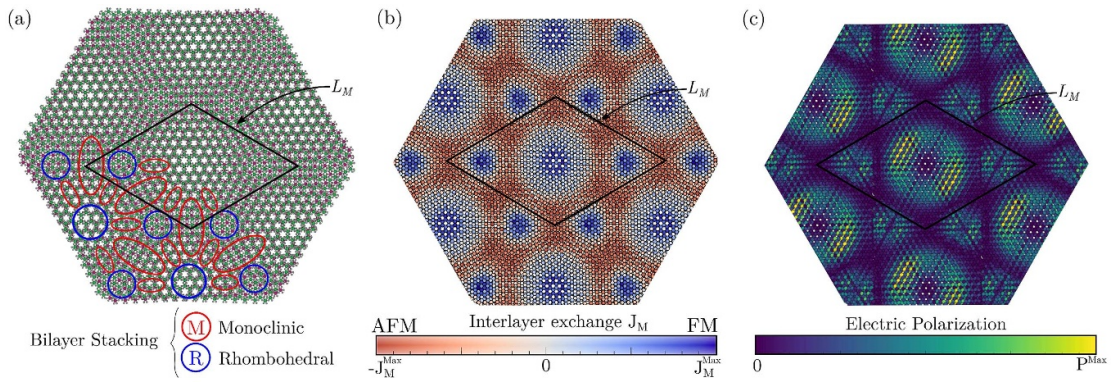

Figure 1. (a) Top view of the twisted CrX_3 bilayer at small angles. Ligand atoms X are represented in gray, and Cr atoms of the bottom (top) layer in pink (green). The moiré unit cell is described by a lattice parameter of the moiré length scale L_M. The emergent moiré pattern leads to regions with monoclinic (M) and rhombohedral (R) stackings, highlighted in red and blue respectively. (b) Moiré profile for the interlayer magnetic exchange J_M originated from the different stackings. The interlayer magnetic exchange interaction is antiferromagnetic (ferromagnetic) in the monoclinic (rhombohedral) stacking. (c) Module of the local electric polarization associated with the moiré ground state spin texture.

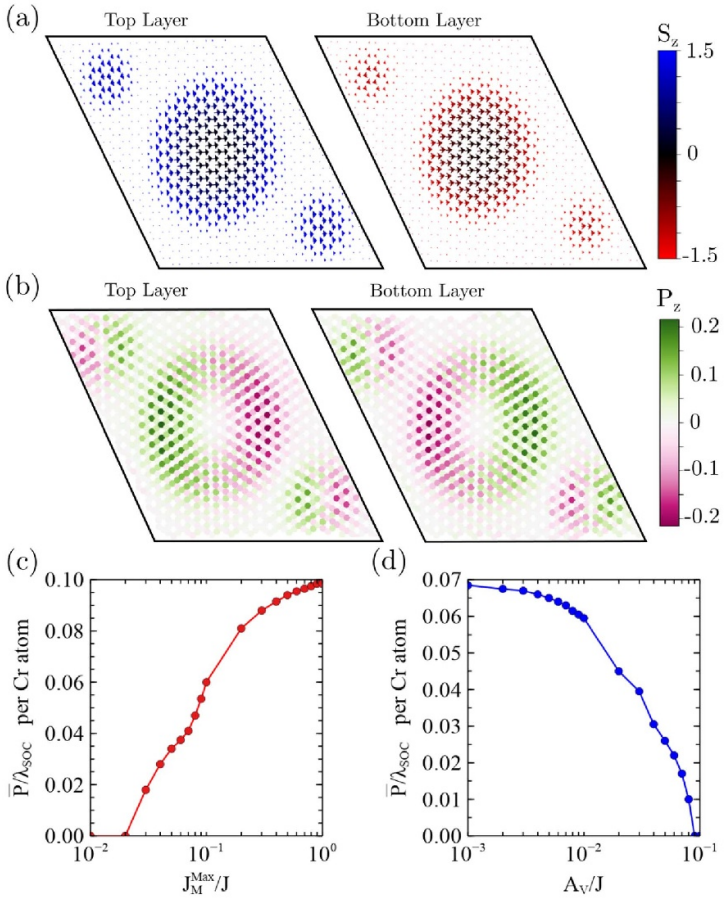

Figure 2. Ground state solution of the spin Hamiltonian for the twisted system. (a) Ground state spin texture on the top (bottom) layer is shown in the left (right) panel. S_x and S_y components are depicted as a vector field. The color of the vectors shows the S_z component. (b) Associated electric polarization (P_z component) to the ground state magnetic texture. (c) Electric polarization average of the ground state as a function of the interlayer exchange maximum J_M^{max} ($A_v/J = 0.01$ and $A_u/J = 0.001$). At low values of J_M^{max} no spin texture is formed. (d) Electric polarization average of the ground state as a function of the anisotropic magnetic exchange A_v ($J_M^{max}/J = 0.1$ and $A_u/J = 0.001$). At high values of A_v no spin texture is formed.

$A_v/J > 0.1$, so CrI_3 would be on the verge of displaying a multiferroic behavior due to its strong uniaxial anisotropy [45].

We now demonstrate and quantify, using density functional theory calculations [62], the emergent electric polarization that we have seen that appears

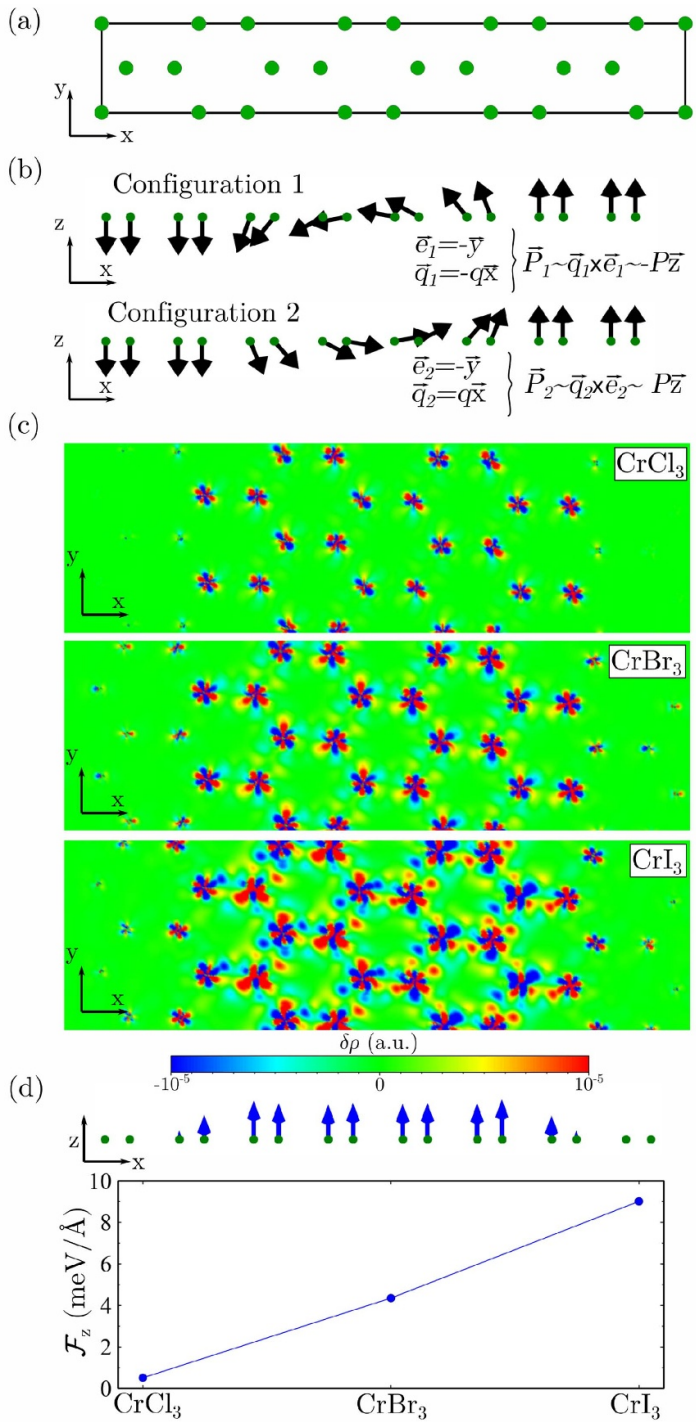

Figure 3. (a) Unit cell used in the *ab initio* calculations, Cr atoms depicted in green, halide atoms omitted for clarity. (b) Equivalent non-collinear magnetic configurations with opposite spin propagation vector **q** and same helicity **e**, and hence opposite electric polarization. (c) Electronic density difference $\delta\rho$ between both equivalent configurations in panel (b) for the three trihalides in the Cr-atoms plane. (d) Force difference between the configurations of the panel (b). A net ferroelectric force emerges in the *z*-direction in the Cr atoms where the magnetism is non-collinear. An average of the ferroelectric force for each trihalide shows the dependence of the electric polarization with the ligand.

in the non-collinear moiré system in virtue of equation (3). Performing first-principles calculations in a full twisted CrX_3 bilayer with spin–orbit coupling and non-collinear magnetism is well beyond the current computational capabilities. However, since the electric polarization arises locally, the *ab initio* analysis can be performed in a system like the one shown in figure 3(a) by imposing a magnetic texture in the CrX_3 layer like the one shown in figure 3(b), that resembles the kind of spin texture found in the ground state between rhombohedric and monoclinic regions. We set the same out-of-plane spin texture to the three compounds to systematically extract the effect of the halide atom and quantification of the

inverse DM interaction [63]. The associated polarization of a non-collinear texture given in equation (3) can be rewritten in terms of a spin spiral propagation vector $\mathbf{q}$ and the spin rotation axis $e = (0, -1, 0)$, leading to an electric polarization of the spin texture [60, 61]

$$\mathbf{P} = \beta \lambda_{SOC} (\mathbf{q} \times \mathbf{e}), \tag{4}$$

where β is a proportionality constant that depends on the electronic structure and crystal environment and are similar for the three compounds. To demonstrate and quantify the emergence of an electric polarization we performed *ab initio* calculations in two equivalent magnetic configurations (figure 3(b)) with the same spin rotation vector $\mathbf{e}$, but with opposite spin propagation vector $\mathbf{q}$. Therefore, an opposite electric polarization will emerge in each of the configurations. The emergence of the electric polarization in the spin texture is directly obtained by taking the difference between the two equivalent configurations. This procedure provides a direct methodology to extract electric polarization stemming from non-collinear magnetic order (see supplementary material). Modifying the q-vector of the spiral, i.e. the size of the supercell, will change the total value of the ferroelectric polarization obtained since it will modify the non-collinear spin order controlling the inverse DM interaction. In our analysis, we use the same spin texture for every chromium trihalide, and hence we can extract the contribution coming from the spin–orbit coupling to the inverse DM interaction.

The emergence of an electric polarization is accompanied by a reconstruction of the electronic density ρ. Therefore, we can analyze the difference in the electronic density $\delta\rho$ between both configurations. This is shown in figure 3(c) for the three chromium halides. We observe that the electronic reconstruction increases by taking a heavier halide. Thus, for the same spin texture, we can see that CrI_3 will produce the strongest ferroelectric polarization. This result is a consequence of the increase of the spin–orbit coupling when one goes down in the halide group, thus demonstrating the effective equations (3) and (4) governed by the SOC prefactor λ_{SOC}.

The reconstruction of the electronic density will lead to the appearance of a ferroelectric force in the atoms in the spin texture in the direction of the emergent electric polarization [10]. Therefore, we can compute the force difference between both configurations in figure 3(b) to provide a direct quantification of the electric polarization in CrX_3. Figure 3(d) shows the force difference between both configurations. We can see that the forces emerge only in the Cr atoms in which the non-collinear magnetism is present. Moreover, we can see that the forces emerge in the z-direction, indicating the direction of the electric dipole, and as expected from the schematic in figure 3(b). We can quantify the dependence on the halide by taking the average of the force module among Cr-atoms for each of the compounds, as shown in 3(d). Taking a heavier halide produces an increase in the ferroelectric force, as expected from the increase of the spin–orbit coupling. As a reference, NiI_2, a 2D multiferroic governed by this same mechanism of spin–orbit coupling and non-collinear magnetism, leads to ferroelectric forces of ≈ 20 meV Å^{-1} [10]. Therefore, this confirms that spin textures produced in twisted CrX_3 bilayers lead to the emergence of an electric polarization with strong magnetoelectric coupling.

We now elaborate on some conclusions on the strength of multiferroic order in twisted CrX_3 bilayers considering together the results obtained from the low energy model and the *ab initio* calculations that allowed us to provide a quantification of the inverse DM interaction in these magnetic moiré systems (see supplementary material). On the one hand, our *ab initio* DFT methods show that as the halide becomes heavier, the ferroelectric polarization becomes stronger. On the other hand, the low energy model shows that the anisotropic exchange has a detrimental impact on the formation of the spin texture and hence on the multiferroic order. In particular, in CrI_3 the strong anisotropic exchange might partially quench the formation of a sizable non-collinear magnetic texture. In $CrCl_3$, the small SOC would yield a comparably weak ferroelectric polarization despite the formation of the non-collinear texture. Therefore, the optimal twisted bilayer that yields the strongest ferroelectric polarization would be $CrBr_3$, or ultimately, a bilayer of an intermediate stoichiometry between $CrBr_3$ and CrI_3 [45].

Finally, we analyze the magnetoelectric coupling present in twisted CrX_3 bilayers [64]. To do so, we now include in the low energy Hamiltonian a coupling to an external electric field $\mathbf{E} = (0, 0, E_z)$ perpendicular to the twisted system in the z-direction

$$\mathcal{H}_E = \frac{1}{2} \sum_{ij} \mathbf{E} \cdot \mathbf{P}_{ij}. \tag{5}$$

We now show how this interlayer bias allows controlling the magnetic order due to the emergent multiferroicity [65]. Figures 4(a) and (b) show the spin texture and the associated electric polarization at $E_z/J = 3$. We can observe that the ground state spin texture shown in figure 2(a) gets significantly modified due to the strong magnetoelectric coupling, leading to the formation of a magnetic skyrmion around the AA rhombohedral stacking in one of the layers [38, 39, 66–72]. Interestingly, such a magnetic state features a non-zero total electric polarization in the z-direction. The evolution of the total electric polarization in the moiré supercell in the z-direction as a function of the external electric field is shown in figure 4(c). The different bumps in P_z as a function of the electric field indicate transitions to different

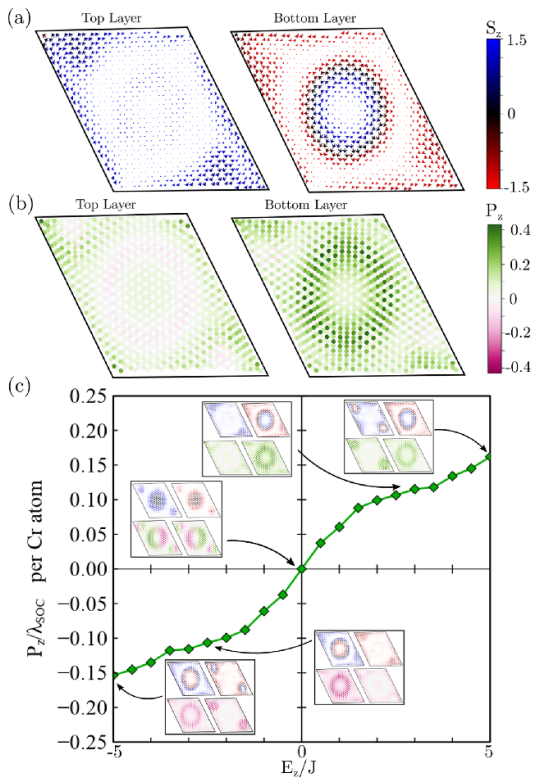

Figure 4. (a) Spin texture in moiré unit cell at $E_z/J = 3$, a magnetic skyrmion emerges in the bottom layer. (b) Associated electric polarization to the spin texture. (c) Evolution of the net electric polarization in the z-direction P_z as a function of the electric field. Different spin textures appear as a function of the electric field: ground state spin texture at $E_z/J = 0$, a magnetic skyrmion appears in the AA stacking area in one of the layers at $E_z/J = \pm 3$, and a second pair of magnetic skyrmions emerge in the other layer around the AB/BA stacking regions at $E_z/J = \pm 5$.

non-trivial spin textures which are shown as insets in figure 4(c). Starting at $E_z/J = 0$ in the ground state spin texture, at $E_z/J = \pm 3$ the magnetic skyrmion shown in figures 4(a) and (b) arises. At $E_z/J = \pm 5$ a second pair of magnetic skyrmions emerge in the other layer around the AB/BA stacking regions (see supplementary material). The critical electric field required to produce a transition to the skyrmionic phase is inversely proportional to the strength of the λ_{SOC}. As a reference, $J \approx 3$ meV and $\alpha\lambda_{SOC} \approx 10^{-4}$e (e electron charge) in twisted $CrBr_3$ bilayers, implying that such magnetic transitions can be experimentally driven via gating at voltages of $1 - 10$ V [65]. This brings twisted $CrBr_3$ bilayers as a promising platform for the electric control of non-trivial magnetic textures, and ultimately as a platform for magnetoelectric skyrmionics.

3. Conclusions

To summarize, we have demonstrated that twisted CrX_3 bilayers develop a multiferroic order due to the interplay between the moiré structure, non-collinear magnetic order, and spin–orbit coupling. We have provided a quantification of the strength of the multiferroic order for this family of compounds, finding that, among the stoichiometric chromium trihalides, $CrBr_3$ is expected to display the strongest multiferroic and magnetoelectric coupling. Furthermore, we have shown that this strong magnetoelectric coupling allows an electrical control of non-trivial magnetic textures using an interlayer bias. Our results put forward a strategy to design a new family of artificial multiferroics with a strong magnetoelectric coupling based on twisted magnetic van der Waals materials.

Data availability statement

All data that support the findings of this study are included within the article (and any supplementary files).

Acknowledgments

We acknowledge the computational resources provided by the Aalto Science-IT project, and the financial support from the Academy of Finland Projects Nos. 331342, 336243 and 349696 and the Jane and Aatos Erkko Foundation. We thank P Liljeroth for useful discussions.

ORCID iDs

Adolfo O Fumega https://orcid.org/0000-0002-3385-6409
Jose L Lado https://orcid.org/0000-0002-9916-1589

References

[1] Hill N A 2000 Why are there so few magnetic ferroelectrics? *J. Phys. Chem.* B **104** 6694–709
[2] Spaldin N A and Ramesh R 2019 Advances in magnetoelectric multiferroics *Nat. Mater.* **18** 203–12
[3] Fiebig M, Lottermoser T, Meier D and Trassin M 2016 The evolution of multiferroics *Nat. Rev. Mater.* **1** 16046
[4] Fiebig M 2005 Revival of the magnetoelectric effect *J. Phys. D: Appl. Phys.* **38** R123–52
[5] Kimura T, Goto T, Shintani H, Ishizaka K, Arima T and Tokura Y 2003 Magnetic control of ferroelectric polarization *Nature* **426** 55–58
[6] Hur N, Park S, Sharma P A, Ahn J S, Guha S and Cheong S-W 2004 Electric polarization reversal and memory in a multiferroic material induced by magnetic fields *Nature* **429** 392–5
[7] Gajek M, Bibes M, Fusil S, Bouzehouane K, Fontcuberta J, Barthélémy Aès and Fert A 2007 Tunnel junctions with multiferroic barriers *Nat. Mater.* **6** 296–302
[8] Nan C-W, Bichurin M I, Dong S, Viehland D and Srinivasan G 2008 Multiferroic magnetoelectric composites: historical perspective, status and future directions *J. Appl. Phys.* **103** 031101
[9] Pantel D, Goetze S, Hesse D and Alexe M 2012 Reversible electrical switching of spin polarization in multiferroic tunnel junctions *Nat. Mater.* **11** 289–93
[10] Fumega A O and Lado J L 2022 Microscopic origin of multiferroic order in monolayer NiI_2 *2D Mater.* **9** 025010
[11] Song Q *et al* 2022 Evidence for a single-layer van der Waals multiferroic *Nature* **602** 601–5

[12] Su Y, Li X, Zhu M, Zhang J, You L and Tsymbal E Y 2020 Van der Waals multiferroic tunnel junctions *Nano Lett.* **21** 175–81
[13] Serlin M, Tschirhart C L, Polshyn H, Zhang Y, Zhu J, Watanabe K, Taniguchi T, Balents L and Young A F 2020 Intrinsic quantized anomalous Hall effect in a moiré heterostructure *Science* **367** 900–3
[14] Geisenhof F R, Winterer F, Seiler A M, Lenz J, Xu T, Zhang F and Thomas Weitz R 2021 Quantum anomalous Hall octet driven by orbital magnetism in bilayer graphene *Nature* **598** 53–58
[15] Li T *et al* 2021 Quantum anomalous Hall effect from intertwined moiré bands *Nature* **600** 641–6
[16] Nuckolls K P, Oh M, Wong D, Lian B, Watanabe K, Taniguchi T, Andrei Bernevig B and Yazdani A 2020 Strongly correlated chern insulators in magic-angle twisted bilayer graphene *Nature* **588** 610–5
[17] Cao Y, Fatemi V, Fang S, Watanabe K, Taniguchi T, Kaxiras E and Jarillo-Herrero P 2018 Unconventional superconductivity in magic-angle graphene superlattices *Nature* **556** 43–50
[18] Oh M, Nuckolls K P, Wong D, Lee R L, Liu X, Watanabe K, Taniguchi T and Yazdani A 2021 Evidence for unconventional superconductivity in twisted bilayer graphene *Nature* **600** 240–5
[19] Kezilebieke S, Huda M N, Vaňo V, Aapro M, Ganguli S C, Silveira O J, Głodzik S, Foster A S, Ojanen T and Liljeroth P 2020 Topological superconductivity in a van der Waals heterostructure *Nature* **588** 424–8
[20] Kezilebieke S, Vaňo V, Huda M N, Aapro M, Ganguli S C, Liljeroth P and Lado J L 2022 Moiré-enabled topological superconductivity *Nano Lett.* **22** 328–33
[21] Park J M, Cao Y, Watanabe K, Taniguchi T and Jarillo-Herrero P 2021 Tunable strongly coupled superconductivity in magic-angle twisted trilayer graphene *Nature* **590** 249–55
[22] Kim H, Choi Y, Lewandowski C, Thomson A, Zhang Y, Polski R, Watanabe K, Taniguchi T, Alicea J and Nadj-Perge S 2022 Evidence for unconventional superconductivity in twisted trilayer graphene *Nature* **606** 494–500
[23] Vaňo V, Amini M, Ganguli S C, Chen G, Lado J L, Kezilebieke S and Liljeroth P 2021 Artificial heavy fermions in a van der Waals heterostructure *Nature* **599** 582–6
[24] Shen S, Wen C, Kong P, Gao J, Si J, Luo X, Lu W, Sun Y, Chen G and Yan S 2022 Inducing and tuning kondo screening in a narrow-electronic-band system *Nat. Commun.* **13** 2156
[25] Ruan W *et al* 2021 Evidence for quantum spin liquid behaviour in single-layer 1T-$TaSe_2$ from scanning tunnelling microscopy *Nat. Phys.* **17** 1154–61
[26] Ugeda M M *et al* 2015 Characterization of collective ground states in single-layer $NbSe_2$ *Nat. Phys.* **12** 92–97
[27] Huang B *et al* 2017 Layer-dependent ferromagnetism in a van der Waals crystal down to the monolayer limit *Nature* **546** 270–3
[28] Yuan S, Luo X, Chan H L, Xiao C, Dai Y, Xie M and Hao J 2019 Room-temperature ferroelectricity in $MoTe_2$ down to the atomic monolayer limit *Nat. Commun.* **10** 1775
[29] Cao Y *et al* 2018 Correlated insulator behaviour at half-filling in magic-angle graphene superlattices *Nature* **556** 80–84
[30] Lu X *et al* 2019 Superconductors, orbital magnets and correlated states in magic-angle bilayer graphene *Nature* **574** 653–7
[31] Polshyn H *et al* 2020 Electrical switching of magnetic order in an orbital chern insulator *Nature* **588** 66–70
[32] Wu F, Lovorn T, Tutuc E, Martin I and MacDonald A H 2019 Topological insulators in twisted transition metal dichalcogenide homobilayers *Phys. Rev. Lett.* **122** 086402
[33] Haavisto M, Lado J L and Otero Fumega A 2022 Topological multiferroic order in twisted transition metal dichalcogenide bilayers *SciPost Phys.* **13** 052
[34] Song T *et al* 2021 Direct visualization of magnetic domains and moiré magnetism in twisted 2D magnets *Science* **374** 1140–4
[35] Wang C, Gao Y, Lv H, Xu X and Xiao Di 2020 Stacking domain wall magnons in twisted van der Waals magnets *Phys. Rev. Lett.* **125** 247201
[36] Xie H *et al* 2021 Twist engineering of the two-dimensional magnetism in double bilayer chromium triiodide homostructures *Nat. Phys.* **18** 30–36
[37] Xu Y *et al* 2021 Coexisting ferromagnetic–antiferromagnetic state in twisted bilayer CrI_3 *Nat. Nanotechnol.* **17** 143–7
[38] Xiao F, Chen K and Tong Q 2021 Magnetization textures in twisted bilayer CrX_3 (X=Br, I) *Phys. Rev. Res.* **3** 013027
[39] Akram M, LaBollita H, Dey D, Kapeghian J, Erten O and Botana A S 2021 Moiré skyrmions and chiral magnetic phases in twisted CrX_3 (X = I, Br and Cl) bilayers *Nano Lett.* **21** 6633–9
[40] Xu Y, Ray A, Shao Y-T, Jiang S, Weber D, Goldberger J E, Watanabe K, Taniguchi T, Muller D A, Fai Mak K and Shan J 2021 Emergence of a noncollinear magnetic state in twisted bilayer CrI_3 (arXiv:2103.09850 [cond-mat.mtrl-sci])
[41] Xie H, Luo X, Ye Z, Ye G, Ge H, Yan S, Fu Y, Tian S, Lei H, Sun K, He R and Zhao L 2022 Evidence of Noncollinear Spin Texture in Magnetic Moiré Superlattices (arXiv:2204.01636 [cond-mat.mtrl-sci])
[42] Lado J L and Fernández-Rossier J 2017 On the origin of magnetic anisotropy in two dimensional CrI_3 *2D Mater.* **4** 035002
[43] Zhang W-B, Qu Q, Zhu P and Lam C-H 2015 Robust intrinsic ferromagnetism and half semiconductivity in stable two-dimensional single-layer chromium trihalides *J. Mater. Chem.* **3** 12457–68
[44] Song K W and Fal'ko V I 2022 Superexchange and spin-orbit coupling in monolayer and bilayer chromium trihalides *Phys. Rev.* B **106** 245111
[45] Tartaglia T A *et al* 2020 Accessing new magnetic regimes by tuning the ligand spin-orbit coupling in van der Waals magnets *Sci. Adv.* **6** 30
[46] Webster L and Yan J-A 2018 Strain-tunable magnetic anisotropy in monolayer $CrCl_3$, $CrBr_3$ and CrI_3 *Phys. Rev.* B **98** 144411
[47] In the absence of strain, $CrCl_3$ shows in-plane anisotropy
[48] Xu C, Feng J, Xiang H and Bellaiche L 2018 Interplay between Kitaev interaction and single ion anisotropy in ferromagnetic CrI_3 and $CrGeTe_3$ monolayers *npj Comput. Mater.* **4** 57
[49] Kartsev A, Augustin M, Evans R F L, Novoselov K S and Santos E J G 2020 Biquadratic exchange interactions in two-dimensional magnets *npj Comput. Mater.* **6** 150
[50] Chen L, Chung J-H, Gao B, Chen T, Stone M B, Kolesnikov A I, Huang Q and Dai P 2018 Topological spin excitations in honeycomb ferromagnet CrI_3 *Phys. Rev.* X **8** 041028
[51] Lu X, Fei R, Zhu L and Yang Li 2020 Meron-like topological spin defects in monolayer $CrCl_3$ *Nat. Commun.* **11** 4724
[52] Sivadas N, Okamoto S, Xu X, Fennie C J and Xiao Di 2018 Stacking-dependent magnetism in bilayer CrI_3 *Nano Lett.* **18** 7658–64
[53] Soriano D, Cardoso C and Fernández-Rossier J 2019 Interplay between interlayer exchange and stacking in CrI_3 bilayers *Solid State Commun.* **299** 113662
[54] Chen W, Sun Z, Wang Z, Gu L, Xu X, Wu S and Gao C 2019 Direct observation of van der Waals stacking–dependent interlayer magnetism *Science* **366** 983–7
[55] Gibertini M 2020 Magnetism and stability of all primitive stacking patterns in bilayer chromium trihalides *J. Phys. D: Appl. Phys.* **54** 064002
[56] Soriano D 2022 Domain wall formation and magnon localization in twisted chromium trihalides *Phys. Status Solidi* **16** 2200078
[57] In the case of $CrCl_3$ the stacking dependence of the interlayer magnetic exchange has not been fully established. *Ab initio* calculations have found a highly functional dependence on the interlayer magnetic exchange [39, 73]. However, it has also been shown, that this interlayer coupling is weak and

external fields, can drive bilayer $CrCl_3$ to the same scenario as the other two halides [73]
[58] A detailed explanation of the interlayer exchange parametrization and the robustness of the results against perturbations to it, such as the twist angle, are included in the supplemental material
[59] Computational details about the minimization procedure to obtain the ground state are included in the supplemental material
[60] Katsura H, Nagaosa N and Balatsky A V 2005 Spin current and magnetoelectric effect in noncollinear magnets *Phys. Rev. Lett.* **95** 057205
[61] Mostovoy M 2006 Ferroelectricity in spiral magnets *Phys. Rev. Lett.* **96** 067601
[62] Hohenberg P and Kohn W 1964 Inhomogeneous electron gas *Phys. Rev.* **136** B864–71
[63] An in-plane spin texture provides results on the same order of magnitude for $CrCl_3$
[64] Importantly, to drive conclusions about the strength of the magnetoelectric coupling we are considering the parameters corresponding to $CrBr_3$, which is found to display the strongest multiferroic order
[65] Cheng G, Rahman M M, Allcca A L, Rustagi A, Liu X, Liu L, Fu L, Zhu Y, Mao Z, Watanabe K, Taniguchi T, Upadhyaya P and Chen Y P 2022 Electrically tunable moiré magnetism in twisted double bilayer antiferromagnets (arXiv:2204.03837 [cond-mat.mtrl-sci])
[66] Tong Q, Liu F, Xiao J and Yao W 2018 Skyrmions in the moiré of van der Waals 2D magnets *Nano Lett.* **18** 7194–9
[67] Ray S and Das T 2021 Hierarchy of multi-order skyrmion phases in twisted magnetic bilayers *Phys. Rev.* B **104** 014410
[68] Hejazi K, Luo Z-X and Balents L 2021 Heterobilayer moiré magnets: Moiré skyrmions and commensurate-incommensurate transitions *Phys. Rev.* B **104** L100406
[69] Hejazi K, Luo Z-X and Balents L 2020 Noncollinear phases in moiré magnets *Proc. Natl Acad. Sci.* **117** 10721–6
[70] Wu Y *et al* 2022 A van der Waals interface hosting two groups of magnetic skyrmions *Adv. Mater.* **34** 2110583
[71] Zheng F 2023 Magnetic skyrmion lattices in a novel 2d-twisted bilayer magnet *Adv. Funct. Mater.* **33** 2206923
[72] Kim K-M, Kiem D H, Bednik G, Han M J and Park M J 2022 Theory of moire magnets and topological magnons: applications to twisted bilayer CrI_3 (arXiv:2206.05264 [cond-mat.str-el])
[73] Klein D R *et al* 2019 Enhancement of interlayer exchange in an ultrathin two-dimensional magnet *Nat. Phys.* **15** 1255–60